Neuron

NeuroResource

Opto-vTrap, an optogenetic trap for reversible inhibition of vesicular release, synaptic transmission, and behavior

Graphical abstract

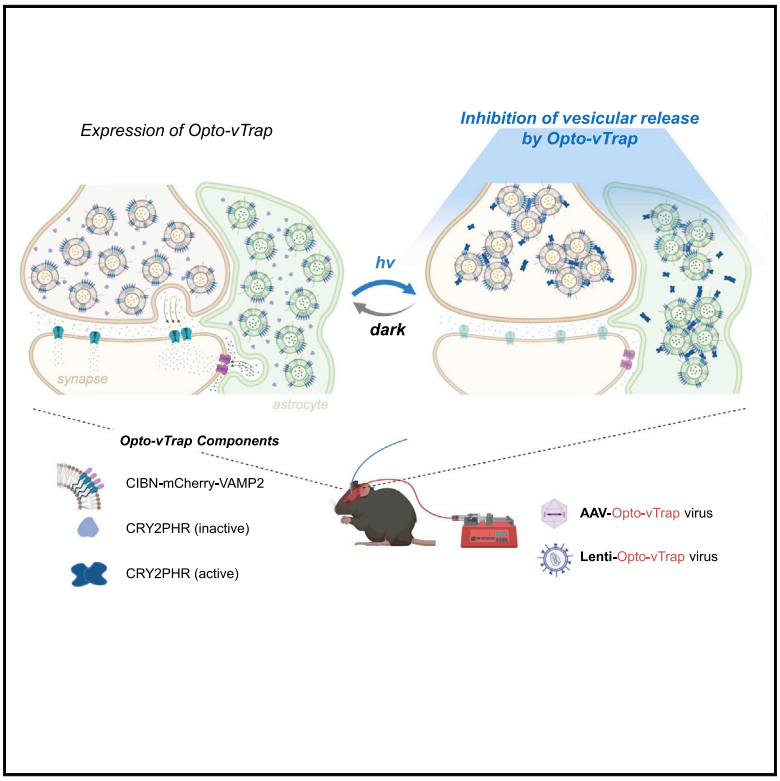

Highlights

- Opto-vTrap is a quickly reversible optogenetic tool for inhibition of vesicular release
- It is a blue-light-induced vesicle-trapping system based on CRY2 and CIBN interaction
- It shows reversible inhibition of synaptic and gliotransmission and behavior.
- Opto-vTrap can be applied broadly in *in vitro*, *ex vivo*, and *in vivo* models

Authors

Joungha Won, Yuriy Pankratov, Minwoo Wendy Jang, ..., Soowon Park, C. Justin Lee, Won Do Heo

Correspondence

cjl@ibs.re.kr (C.J.L.),
wondo@kaist.ac.kr (W.D.H.)

In brief

Won et al. engineered Opto-vTrap, a light-inducible and quickly reversible inhibition system to temporarily trap transmitter-containing vesicles from vesicular exocytosis. Opto-vTrap can be used widely in cells, brain slices, and animal behavioral experiments with fast recovery and without affecting membrane potential.

Won et al., 2022, Neuron *110*, 423–435
February 2, 2022
https://doi.org/10.1016/j.neuron.2021.11.003

CellPress

Neuron

CellPress

NeuroResource

Opto-vTrap, an optogenetic trap for reversible inhibition of vesicular release, synaptic transmission, and behavior

Joungha Won,[1,2] Yuriy Pankratov,[3] Minwoo Wendy Jang,[1,4] Sunpil Kim,[1,4] Yeon Ha Ju,[1] Sangkyu Lee,[1] Seung Eun Lee,[5] Arie Kim,[1] Soowon Park,[1] C. Justin Lee,[1,4,*] and Won Do Heo[1,2,6,7,*]

[1]Center for Cognition and Sociality, Institute for Basic Science (IBS), Daejeon 34126, Republic of Korea
[2]Department of Biological Sciences, Korea Advanced Institute of Science and Technology (KAIST), Daejeon 34141, Republic of Korea
[3]School of Life Sciences, University of Warwick, Coventry, CV4 7AL, UK
[4]KU-KIST Graduate School of Converging Science and Technology, Korea University, Seoul 02841, Republic of Korea
[5]Virus Facility, Research Animal Resource Center, Korea Institute of Science and Technology (KIST), Seoul 02792, Republic of Korea
[6]KAIST Institute for the BioCentury, Korea Advanced Institute of Science and Technology (KAIST), Daejeon 34141, Republic of Korea
[7]Lead contact
*Correspondence: cjl@ibs.re.kr (C.J.L.), wondo@kaist.ac.kr (W.D.H.)
https://doi.org/10.1016/j.neuron.2021.11.003

SUMMARY

Spatiotemporal control of brain activity by optogenetics has emerged as an essential tool to study brain function. For silencing brain activity, optogenetic probes, such as halorhodopsin and archaerhodopsin, inhibit transmitter release indirectly by hyperpolarizing membrane potentials. However, these probes cause an undesirable ionic imbalance and rebound spikes. Moreover, they are not applicable to use in non-excitable glial cells. Here we engineered Opto-vTrap, a light-inducible and reversible inhibition system to temporarily trap the transmitter-containing vesicles from exocytotic release. Light activation of Opto-vTrap caused full vesicle clusterization and complete inhibition of exocytosis within 1 min, which recovered within 30 min after light off. We found a significant reduction in synaptic and gliotransmission upon activation of Opto-vTrap in acute brain slices. Opto-vTrap significantly inhibited hippocampus-dependent memory retrieval with full recovery within an hour. We propose Opto-vTrap as a next-generation optogenetic silencer to control brain activity and behavior with minimal confounding effects.

INTRODUCTION

Understanding brain circuits that are activated or silenced by releasing and receiving molecules between brain cells is a major challenge to neuroscience. During the fast functional information transfer between neuron and neuron or glia and neuron, transmitters are released by calcium-triggered vesicular exocytosis (Harada et al., 2016; Parpura and Zorec, 2010; Südhof, 2012). There has been a considerable research effort to develop tools for modulating brain activity from the cellular level to behaving animals. To spatially, temporally, and cell-type-specifically modulate brain circuits, optogenetic strategies have emerged. The light-gated cation channel channelrhodopsin-2 (ChR2) is used widely for stimulating brain networks by depolarizing membrane potential followed by illumination (Boyden et al., 2005; Lin et al., 2009; Nagel et al., 2003). Activated ChR2 increases calcium influx through the gate of ChR2 and voltage-gated calcium channels, and it causes release of transmitters (Schoenenberger et al., 2011). Optogenetic tools for stimulating neuronal activity, such as ChR2, ChR2 variants, and others, typically utilize cation channels that depolarize membrane potential (Nagel et al., 2003).

Optogenetic tools for inhibiting neuronal activity, such as halorhodopsin (NpHR), archaerhodopsin (Arch), and anion-conducting channelrhodopsin have become popular. NpHR and Arch utilize light-inducible chloride or proton pumps that hyperpolarize membrane potential (Chow et al., 2010; Zhang et al., 2007). Although light activation of NpHR and Arch efficiently silence neuronal activity within a short time, prolonged activation results in critically confounding responses (Wiegert et al., 2017). For instance, prolonged activation of NpHR causes accumulation of intracellular chloride ions and $GABA_A$ reversal potential shift, which results in inadvertent excitatory responses to GABA (Raimondo et al., 2012). In addition, NpHR-mediated hyperpolarization causes recovery from inactivation of low-voltage-activated T-type calcium channels, which are subsequently activated upon light-off, resulting in unintended burst firing (Mahn et al., 2016; Mattingly et al., 2018; Weiss et al., 2012). Furthermore, activation of Arch causes a decrease in intracellular proton concentration or high pH, which has a profound effect on various cellular pathways, such as an increase in calcium concentration and neurotransmitter release (Mahn et al., 2016). Because of these critical issues, many researchers have turned away from NpHR and Arch and started to prefer chemogenetic approaches, such as G_i designer receptors exclusively activated by designer drugs (G_i-DREADDs) (Armbruster et al., 2007). However, G_i-DREADDs also suffer from the same

issue of unintended burst firing upon activation in addition to other disadvantages, such as slow drug onset and offset kinetics (Saloman et al., 2016; Wiegert et al., 2017). Last, NpHR and Arch are not applicable to non-excitable glial cells, such as astrocytes. Because of these shortcomings, there is a pressing need to develop advanced optogenetic silencers without affecting membrane potential.

To circumvent the shortcomings of manipulating membrane potential, optogenetic and chemogenetic tools that directly target and disrupt the synaptic vesicular release machinery have been considered (Karpova et al., 2005; Lin et al., 2013; Liu et al., 2019). The synaptic vesicle release machinery includes soluble N-ethylmaleimide-sensitive fusion attachment protein receptor (SNARE) complex-mediated vesicle docking and priming, complexin binding to the SNARE complex, and calcium binding to synaptotagmin-1 and zippering the SNARE complex to form a pore for vesicle fusion (Rizo and Xu, 2015; Sudhof, 2004; Zhou et al., 2017). The SNARE complex is composed of the highly conserved vesicular SNARE (v-SNARE), including VAMP2 (Synaptobrevin2), and target plasma membrane SNARE (t-SNARE), including syntaxin-1 and SNAP25 (Söllner et al., 1993). To optogenetically target and disrupt vesicular release machinery, Lin et al. (2013) introduced chromophore-assisted light inactivation (CALI)-based synaptic inhibition (InSynC). This system utilizes light-dependent generation of singlet oxygen that damages v-SNARE and disrupts synaptic vesicle release. However, this system has a serious off-target effect because the generated singlet oxygens can diffuse and permanently destroy nearby proteins. Recently reported photo-activable botulinum neurotoxin (PA-BoNT) overcomes this limitation by directly cleaving VAMP2 upon illumination (Liu et al., 2019). However, PA-BoNT has a very long recovery time of about 24 h in *C. elegans*, possibly because it takes a long time for the cleaved VAMP2 to be replenished either by *de novo* protein synthesis or by lateral trafficking from undamaged VAMP2 (Liu et al., 2019). InSynC has a similarly long recovery time because of slow replenishment of the damaged proteins. The long recovery time usually imposes a time constraint on the type of experiments that can be performed; for example, short-duration behavioral tests, such as novel object recognition, object place recognition, five-trial social interaction, and fear conditioning and extinction, cannot be performed with an optogenetic tool having a 24-h recovery time. Therefore, it is necessary to develop a novel optogenetic tool that disrupts the vesicular release machinery at a fast recovery time.

In response to this growing need, we designed and developed Opto-vTrap, a quickly reversible optogenetic inhibition system for direct inhibition of vesicular exocytosis. This system directly targets and sequesters transmitter-containing vesicle into the vesicle cluster and inhibits vesicular release. Unlike the G_i-DREADD system, Opto-vTrap quickly activates and recovers by using light-inducible on and off. Unlike NpHR or Arch, this system does not induce membrane potential change, and Opto-vTrap has a much faster recovery than other vesicle-targeting optogenetic probes. We employed the recently characterized light-activated reversible inhibition by assembled trap (LARIAT) (Lee et al., 2014) to directly target and reversibly disrupt the vesicular release machinery. LARIAT utilizes the property of blue light-inducible heteromerization between cryptochrome 2 (CRY2) from *Arabidopsis thaliana* and cryptochrome-interacting basic-helix-loop-helix 1 (CIB1), which has subsecond time resolution and fast reversibility within minutes (Kennedy et al., 2010). With this property, LARIAT sequesters a target protein by forming a CRY2-CIB1 multimeric complex (Kennedy et al., 2010; Lee et al., 2014). Here we show that Opto-vTrap effectively and reversibly traps synaptic vesicles in neurons as well as gliotransmitter-containing vesicles in astrocytes. We further show that Opto-vTrap can be used widely in cells, brain slices, and animal behavioral experiments, recovering quickly and without affecting membrane potential.

RESULT

Engineering Opto-vTrap, a LARIAT-based vesicle-trapping system

To directly target and reversibly disrupt the vesicular release machinery, we newly designed Opto-vTrap, a light-inducible vesicle-trapping system based on LARIAT (Figure 1A). LARIAT is composed of two critical components: the light-responsive CRY2 and its target protein CIB1, which is conjugated with a multimeric protein of interest (Figure 1A). CRY2 reversibly and strongly interacts with CIB1 to form a CRY2:CIB1 heterodimer and clusters with other CRY2s (CRY2:CRY2) to form homomeric oligomers upon blue light illumination (Bugaj et al., 2013; Rosenfeldt et al., 2008). To increase the efficiency of light-induced vesicle trapping through heteromeric dimer and homomeric oligomer formation, we tried to reduce the size of CIB1 and CRY2 by using the shortened versions of the N-terminal photolyase homology region (PHR) domain (amino acids 1–498) of CRY2 and the C-terminal truncated version (amino acids 1–170) of CIB1 (CIBN) (Kennedy et al., 2010; Figure 1A) (hereafter, CRY2 denotes this shortened version of the PHR domain [amino acids 1–498] of CRY2). To optically trap vesicles, we conjugated CIBN with the v-SNARE protein VAMP2 (Figure 1A), which interacts with t-SNARE proteins such as SNAP25 and syntaxin-1 (Hastoy et al., 2017; Hayashi et al., 1994; Lin et al., 2013; Schoch et al., 2001). As a fluorescent reporter, we inserted mCherry between CIBN and VAMP2 (Figure 1A) because it has been shown that tagging a fluorescent protein to the cytosolic N terminus or lumenal C terminus of VAMP2 does not interfere with VAMP2 function during exocytosis (Deák et al., 2006). For CRY2, we conjugated it with mCitrine as a fluorescent reporter (Figure 1A). Thus, Opto-vTrap was composed of two molecular components in the overexpression vector (pcDNA3.1), each containing CMV::CIBN-mCherry-VAMP2 (CIBN-VAMP2) and CMV::CRY2PHR-mCitrine (CRY2) (Figure 1A). Upon blue light (~488 nm) illumination of Opto-vTrap, CRY2 responds by forming heteromeric dimers of CRY2:CIBN-VAMP2 and homomeric oligomers of CRY2:CRY2 (Figure 1B).

To visualize and test whether Opto-vTrap clusters intracellular vesicles upon light stimulation, we co-expressed CIBN-VAMP2 and CRY2 in Cos-7 cells and measured the movement of vesicles. We used a blue laser to stimulate Opto-vTrap and examined the clustering of vesicles using confocal microscopy (Figure 2B). Before blue light illumination, CIBN-VAMP2 and CRY2 signals were distributed diffusely in the cytosol (Figures 2B, left panel, 2I, and 2J). However, upon illumination with the blue laser

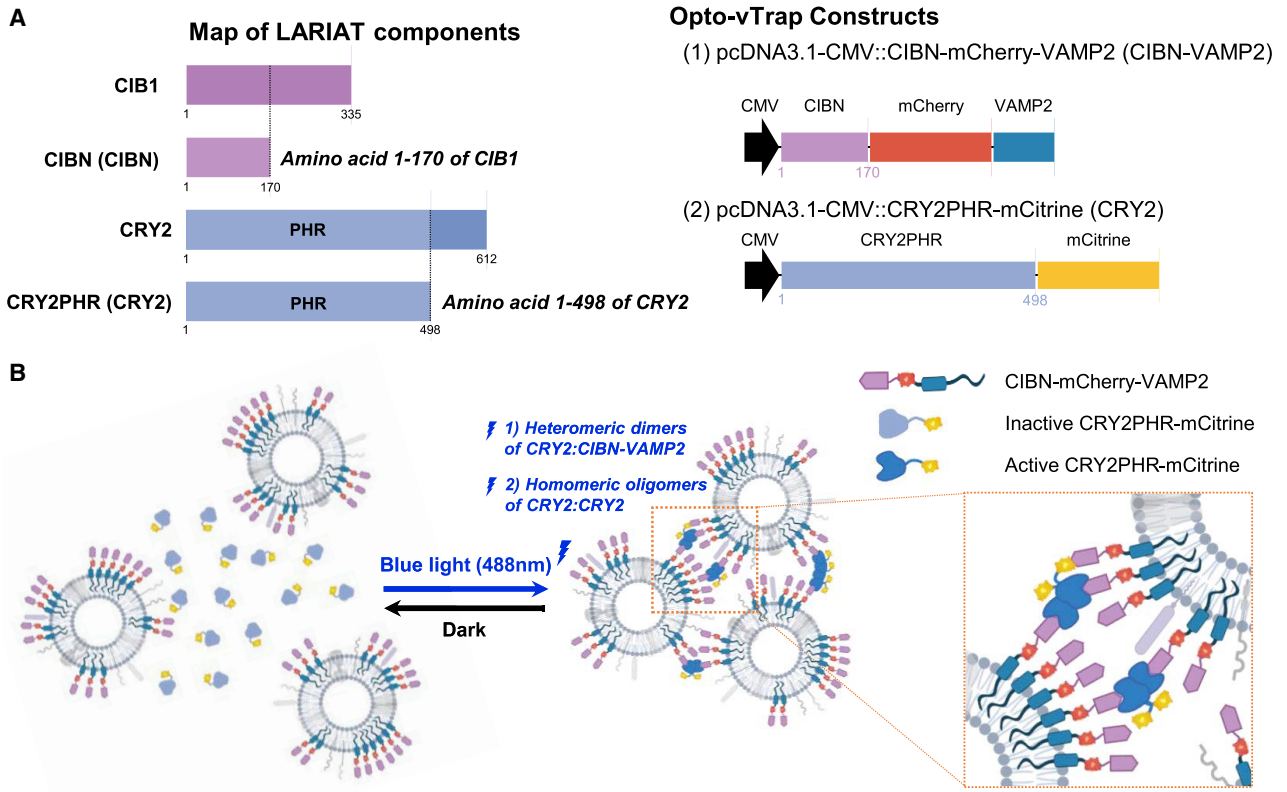

Figure 1. Design and principles of Opto-vTrap

(A) Map of LARIAT components and the Opto-vTrap constructs.

(B) Experimental scheme of the working principle of Opto-vTrap. Blue light (488 nm) illumination triggers heteromeric dimerization of CRY2:CIBN-VAMP and homomeric oligomerization of CRY2:CRY2 and induces vesicle clusterization. Thus, CIBN-VAMP2 targeting vesicles are reversibly clusterized upon blue light illumination.

at 0.2 Hz and a 20% duty cycle (1-s exposure, 4 s off, at 5-s intervals), we observed simultaneous clustering of CIBN-VAMP2 and CRY2 within 5 min and throughout illumination, which recovered fully 15 min after laser-off (Figure 2B). The time course of the line intensity image along the yellow arrow in Figure 2B shows a detailed time course of CIBN-VAMP2 and CRY2 clustering and recovery (Figures 2C and 2D). We observed immediate clustering within 2 min and much slower declustering, which took about 15 min to recover fully (Figure 2D). We also observed that the relative number of CIBN-VAMP2 puncta was increased within 2 min of laser-on (Figures 2E–2G) and recovered slowly after 15 min of laser-off (Figures 2E–2G). To determine the time course of the clustering between CIBN-VAMP2 and CRY2, we calculated the Pearson's correlation coefficient at each time point and found that the value of the coefficient increased steeply with a time constant of $\tau = 10.9$ s, plateaued after 60 s (Figure 2H), and decreased exponentially with $\tau = 543.9$ s (Figure 2J). These results indicate that the two components of Opto-vTrap cluster quickly within 1 or 2 min upon light stimulation and recover slowly within 15 min after stimulation-off.

Opto-vTrap impaired vesicular exocytosis

To examine whether Opto-vTrap impairs vesicular exocytosis upon light stimulation, we performed total internal reflection fluorescence (TIRF) imaging to visualize individual exocytotic events (Becherer et al., 2007). To visualize exocytotic events, we expressed Opto-vTrap in Neuroscreen-1 (NS-1) cells together with neuropeptide-Y (NPY)-VENUS (NPY tagged with VENUS pH-insensitive fluorescent protein) (Figure 3A). To induce exocytosis, we applied a high-potassium solution (70 mM KCl) 30 s after the start of 488 nm blue light stimulation at 5 Hz and a 40% duty cycle (80 ms exposure, 120 ms off, at 200 ms intervals) (Figure 3B). The 488-nm laser simultaneously activated Opto-vTrap and visualized NPY-VENUS under TIRF imaging (Figure 3B). Under the control condition (without CRY2), we observed that numerous spots of about 1 μm size appeared upon high potassium application, which were totally absent under the Opto-vTrap condition (Figures 3C and 3D), indicating that light stimulation of Opto-vTrap abolished exocytosis of NPY-VENUS-containing vesicles. Detailed analysis of each exocytotic event measured by fluorescence intensity (Figure 3D) showed that KCl-induced exocytotic events occur quickly after KCl application under the control condition but not under the Opto-vTrap condition (Figure 3E). The peak amplitude fluorescence intensity during exocytosis was eliminated completely by light stimulation of Opto-vTrap (Figure 3F). These results indicate that Opto-vTrap effectively blocks vesicular exocytosis.

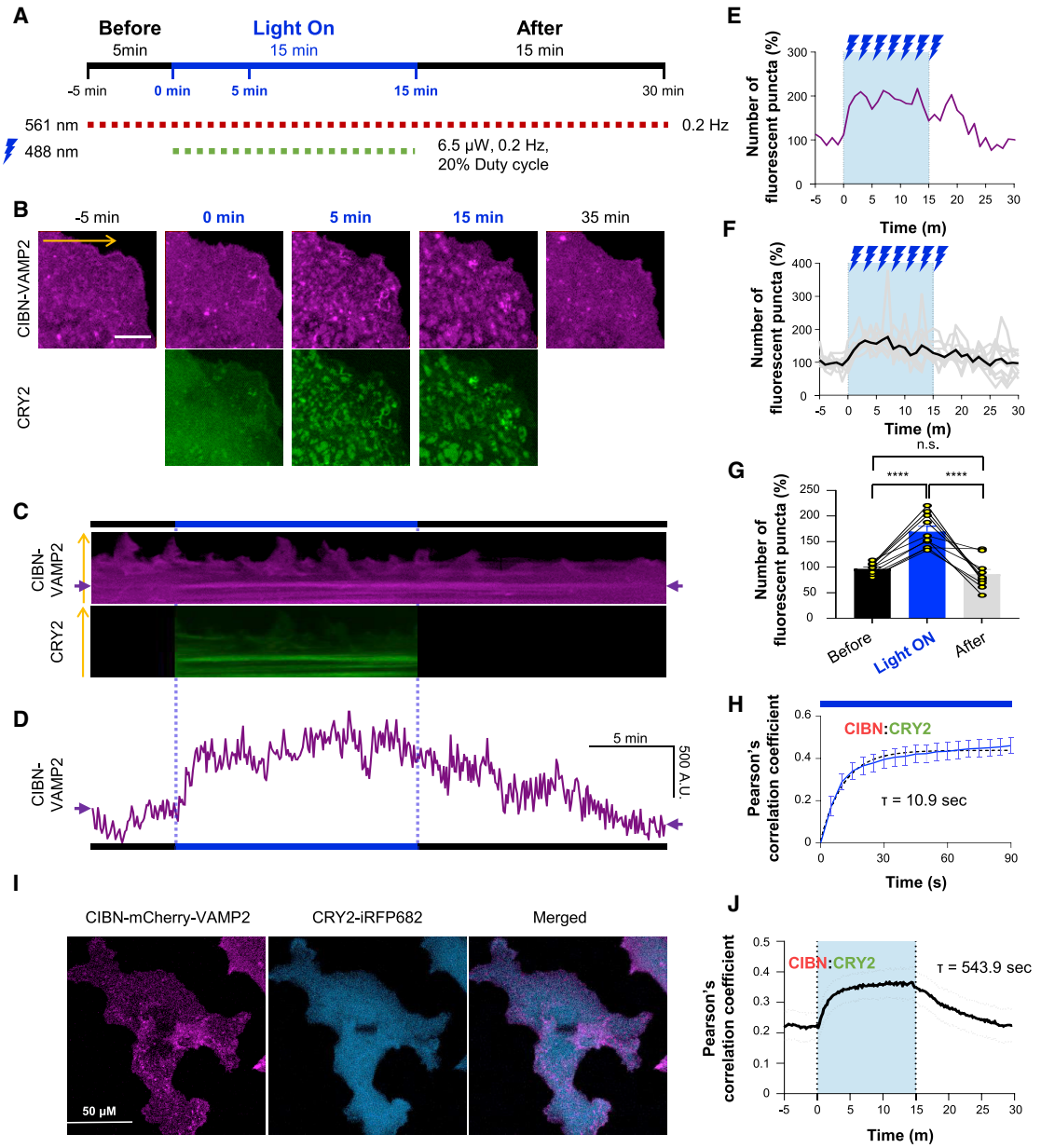

Figure 2. Characterization of Opto-vTrap in COS-7 cells

(A) Experimental timeline and scheme of live-cell imaging of Opto-vTrap. A 488-nm blue laser was turned on (light on) for 15 min. A 561-nm laser was used for CIBN-VAMP2 detection. A 0.2 Hz of 20% duty cycle of 488 nm laser was used for Opto-vTrap activation and CRY2 detection.

(B) Confocal images of Opto-vTrap (CIBN-mCherry-VAMP2 and CRY2-mCitrine)-expressing COS-7 cells. The yellow arrow indicates the position of the kymograph depiction in (C).

(C) The kymograph of CIBN-VAMP2 through the yellow arrow drawn in (B). Magenta arrows indicate the position of the intensity profile depiction in (D). The timing of the 488-nm laser is represented as a blue line.

(D) The intensity profile of CIBN-VAMP2 through the magenta arrows from the kymograph in (C).

(E) Representative quantification graph of the number of vesicle puncta in (B). The blue box indicates 488-nm laser illumination for Opto-vTrap activation.

(F) Individual (gray) and averaged (black) quantification graphs of the number of vesicle puncta.

(G) Percentage of CIBN-VAMP2 fluorescent puncta before, during light on, and 15 min after light off (after) (before, averaged number of puncta in 0–5 min; light on, maximum value during light on; after, averaged number of puncta at 25–30 min, respectively) (n = 10; data are presented as the mean ± SEM. ****$p < 0.0001$, one-way ANOVA test).

(H) Pearson's correlation coefficient (blue line) between CIBN-VAMP2-mCherry and CRY2-mCitrine after blue laser on (n = 10, data are presented as the mean ± SEM) and non-linear fitting curve (black, one-phase association).

(legend continued on next page)

Activation of Opto-vTrap does not affect membrane potential

To examine whether Opto-vTrap activation affects membrane potential, we constructed a lentiviral Opto-vTrap vector containing CRY2PHR-P2A-CIBN-mCherry-VAMP2 under the Ca^{2+}/calmodulin-dependent protein kinase IIα (CamKIIα) promoter and bilaterally injected the lentivirus into the CA3 hippocampus (Figure 4A). We then recorded membrane potential changes in Opto-vTrap-expressing CA3 pyramidal neurons of the acutely prepared hippocampal slices, with current steps ranging from −100 pA to +40 pA (Figure 4B). Immediately after the current steps, we measured changes in membrane potential upon continuous blue light stimulation onto the CA3 region (Figure 4C). We observed that continuous blue light illumination for 10 min did not cause any membrane potential change (Figures 4C and 4D). These results indicate that activation of Opto-vTrap does not affect membrane potential.

Activation of Opto-vTrap inhibits evoked EPSCs in Schaffer collateral synapses

To test whether activation of Opto-vTrap can selectively inhibit synaptic transmission in Schaffer collateral synapses, we recorded evoked excitatory postsynaptic currents (eEPSCs) from CA1 pyramidal neurons while electrically stimulating the Schaffer collateral pathway (Amaral and Witter, 1989) with paired-pulse electrical stimulation (Figure 4E). After establishing a stable baseline of the eEPSC amplitude, we turned 300 μW of continuous blue light onto the CA1 region, near the patch-clamped cell (Figure 4E). We observed that, under the control condition without virus injection, light stimulation did not cause any changes in the first eEPSC, second eEPSC, or paired-pulse ratio (Figures 4F–4L), suggesting no detrimental effect of illumination on synaptic transmission. In addition, there was no significant difference between the control and Opto-vTrap-expressing group in eEPSC amplitude, miniature EPSC (mEPSC) amplitude, and frequency before light illumination (Figure 4F; Figures S3A–S3D). There was no significant difference between the control and Opto-vTrap-expressing groups in action potential firing frequency during current injection, action potential (AP) threshold, and input resistance (Figures S1A–S1D). Furthermore, biogenesis of vesicle and presynaptic volume was not affected by Opto-vTrap expression (Figures S1E–S1H). These results indicate that overexpression of Opto-vTrap has no activity in the absence of light stimulation. In contrast, the Opto-vTrap-injected condition showed a significant reduction of the first eEPSC amplitude and second eEPSC amplitude after 15 min of light-on (Figure 4G-J). In addition, we constructed adeno-associated virus (AAV) Opto-vTrap under the CK(0.4) promoter, which is a short version (0.4 kb) of the CamKIIα promoter (8.5 kb) (Dittgen et al., 2004), and tested it in Schaffer collateral synapses (Figure S4A). We observed an approximately 50% reduction of the first and second eEPSC amplitudes within 10 min of light-on (Figures S4B–S4F). AAV-Opto-vTrap improved about 5% of inhibition efficiency and about 5 min of onset speed over lentiviral Opto-vTrap. In addition to eEPSCs, the frequency of mEPSCs was reduced after 15 min of light-on under the Opto-vTrap-injected condition (Figure S3). The first and second amplitudes were fully recovered within 30 min after light-off (Figures 4G–4J). These results indicate that Opto-vTrap can effectively and reversibly inhibit neurotransmitter release in the brain circuit. Interestingly, activation of Opto-vTrap did not change the paired-pulse ratio (PPR) (Figures 4K and 4L), which is a conventional marker for changes in presynaptic release probability (Dobrunz and Stevens, 1997). The PPR showed no significant difference before, during, and after light-on conditions (Figures 4K and 4L). One of the factors that induces changes in PPR is a change in residual Ca^{2+} in the presynaptic terminal (Dobrunz and Stevens, 1997). Therefore, no change in the PPR (Figure 4K and 4L) suggests that inhibition of vesicular release by Opto-vTrap may not influence presynaptic residual Ca^{2+}.

Activation of Opto-vTrap inhibits neocortical astrocytic vesicular gliotransmitter release

To test whether Opto-vTrap can selectively inhibit vesicular release in non-excitable cells such as astrocytes, we constructed a lentiviral vector containing Opto-vTrap, CRY2PHR-P2A-CIBN-mCherry-VAMP2, under a compact glial fibrillary acidic protein (GFAP) promoter, GfaABC1D (Lee et al., 2008), and injected the lentivirus into layer 2/3 of the neocortex (hereafter, "GFAP promoter" denotes the GfaABC1D promoter) (Figure 5A). We recorded NMDA receptor (NMDAR)-mediated spontaneous current activities in layer 2/3 neurons that were near Opto-vTrap-expressing astrocytes in acutely prepared cortical slices (Figure 5A). To selectively activate astrocytes, we applied TFLLR, a selective agonist of PAR1, a G_i- and G_q-coupled GPCR that causes a Ca^{2+} increase in astrocytes (Hollenberg et al., 1997). It has been demonstrated that PAR1 activation induces TREK-1-mediated fast and Best1-mediated slow glutamate release in the hippocampus CA1 (Woo et al., 2012). In cortical layer 2/3 neurons, we found three types of NMDAR-mediated spontaneous transient inward currents, characterized by decay time kinetics: neuronal mEPSC with a decay time of 20 ms (blue circles), glia-induced fast currents (gFICs) with a decay time of 40–45 ms (orange squares), and glia-induced slow currents (sFICs) with a decay time of 100–300 ms (green triangles) (Figures 5B and 5C). We found that all types of currents were inhibited by D-AP5, but only gFICs and gSICs were inhibited by ifenprodil, suggesting that they are mediated by GluN2B-containing extrasynaptic NMDARs (Figures 5C and 5D). TFLLR application did not cause any change in the frequency of mEPSCs (Figure 5D), whereas TFLLR caused a significant increase in the frequency of gFICs and gSICs under the control condition (Figure 5D). In acute slices of the control group, we observed that, although baseline and TFLLR-induced gFICs were blocked by the astrocytic intracellular vesicle release inhibitor tetanus neurotoxin light chain (TeNTx), baseline and TFLLR-induced gSICs were blocked by the TREK-1 blocker spadin (Figure 5E). In GFAP::Opto-vTrap-injected mice, we observed that

(I) Representative confocal images of Opto-vTrap (CIBN-mCherry-VAMP2 and CRY2-iFRP)-expressing COS-7 cells.
(J) Pearson's correlation coefficient (black line) between CIBN-VAMP2-mCherry and CRY2-iRFP682. The blue box indicates 488-nm laser illumination (n = 8, data are presented as the mean ± SEM).

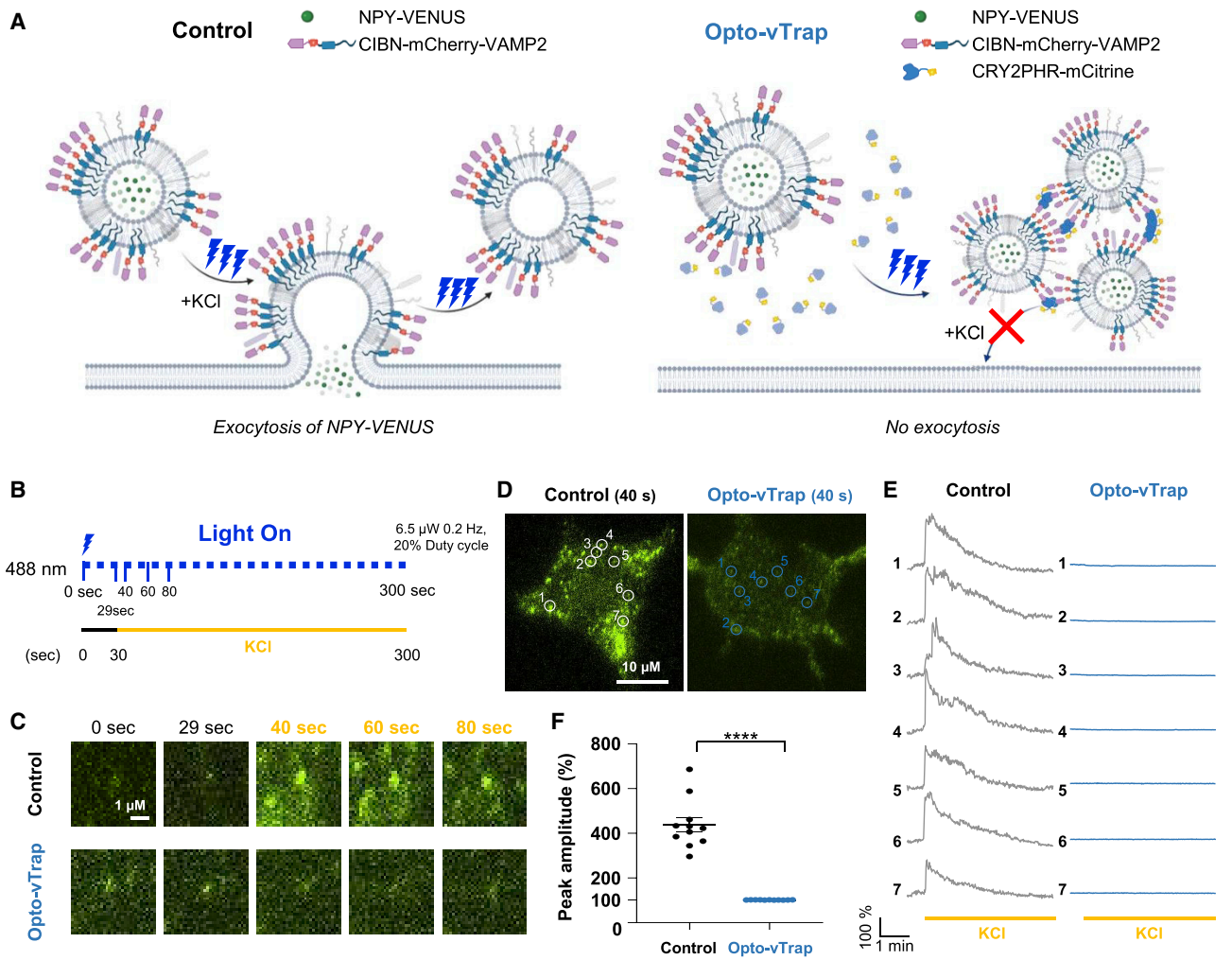

Figure 3. Optogenetic inhibition of vesicular exocytosis by Opto-vTtrap in Neuroscreen-1 cells

(A) Experimental scheme of vesicular exocytosis imaging under TIRF microscopy. In the control, CIBN-VAMP2 and NPY-VENUS were expressed. In Opto-vTrap, CIBN-VAMP2, CRY2, and NPY-VENUS were expressed. NPY-VENUS was used as vesicle content. Exocytosis events were triggered by high-KCl Ringer's solution.

(B) Experimental timeline of vesicle exocytosis imaging under TIRF microscopy. A 5 Hz of 40% duty cycle of 488 nm laser was used for NPY-VENUS detection and Opto-vTrap activation.

(C) Representative TIRF microscopy images of control and Opto-vTrap-expressing Neuroscreen-1 cells. Green signals represent NPY-VENUS.

(D) Representative images of control and Opto-vTrap-expressing Neuroscreen-1 cells 10 s after treatment with high-KCl Ringer's solution. Each circle indicates NPY-VENUS-containing vesicles analyzed in (E).

(E) Representative traces of NPY-VENUS in control and Opto-vTrap-expressing Neuroscreen-1 cells from Figures 2B–2D.

(F) Summary graph of percent peak amplitude of NPY-VENUS puncta in control and Opto-vTrap-expressing Neuroscreen-1 cells after high-KCl solution treatment (n = 11; data are presented as the mean ± SEM; ****$p < 0.0001$, Mann-Whitney test).

the TFLLR-induced increase in the frequency of gFICs was prevented completely by 300 μW of continuous blue light illumination, which recovered fully 15 min after light-off (Figures 5F and 5G), indicating that gFICs are mediated by a vesicular release mechanism. In contrast, the TFLLR-induced increase in the frequency of gSICs was not affected by illumination (Figures 5F and G), indicating that gSICs are mediated by a non-vesicular, channel-mediated release mechanism. These results indicate that Opto-vTrap can be utilized as a fast and reversible optogenetic inhibition tool for vesicular gliotransmitter release.

Activation of Opto-vTrap reversibly inhibits contextual fear memory retrieval

As a final test, we investigated whether activation of Opto-vTrap can inhibit behavior, i.e., hippocampus-dependent contextual memory. The hippocampus has long been implicated in spatial and contextual processing of fear memory (Arias et al., 2015; Fanselow and LeDoux, 1999; Kim and Fanselow, 1992). Hippocampal CA3-CA1 synaptic plasticity is modulated during memory acquisition, extinction, retrieval, and reconditioning of associative learning in an activity-dependent manner (Gruart

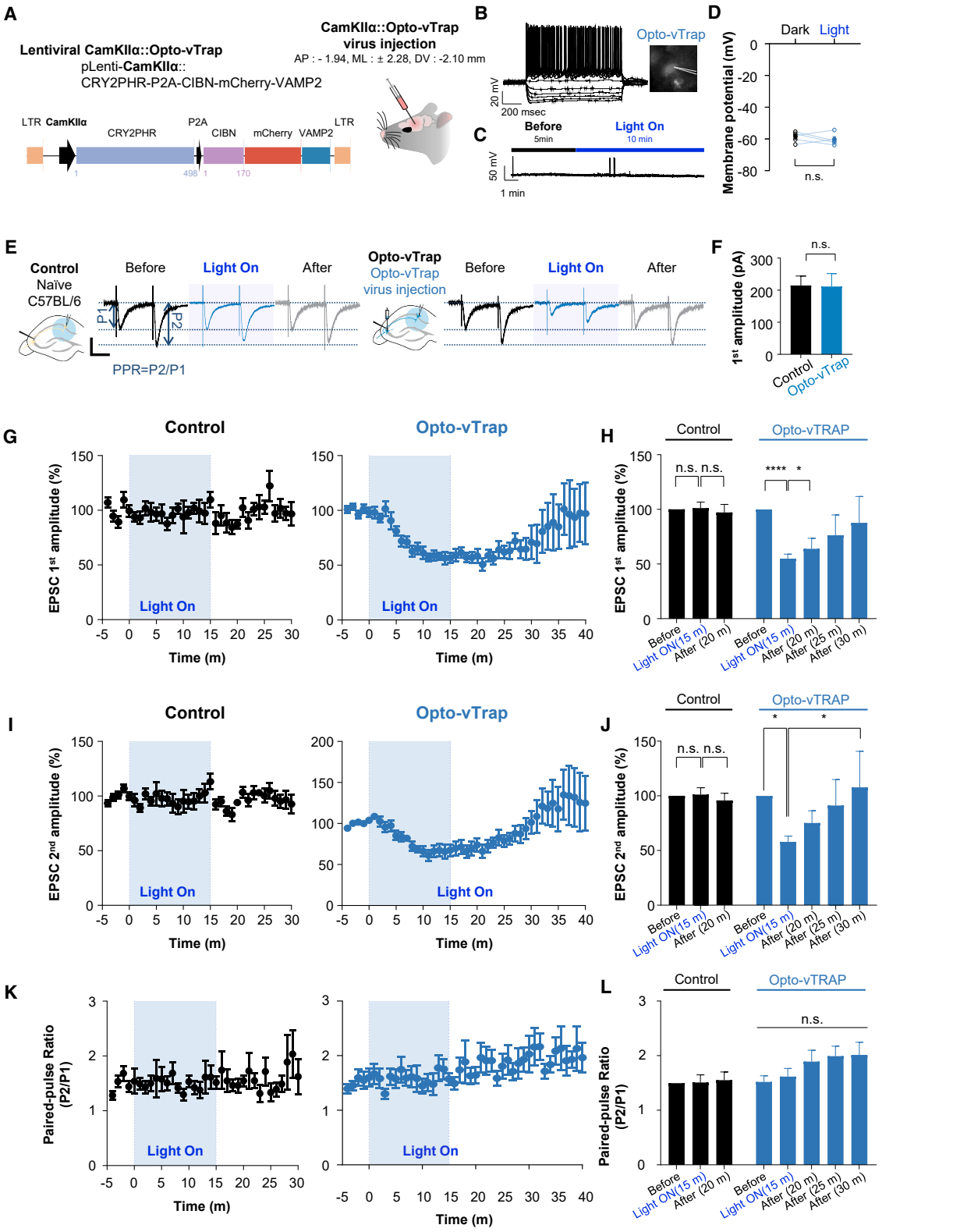

(legend on next page)

et al., 2006). Because it has been reported that lesions of the hippocampal CA3 region cause impaired spatial memory retention in a rat model (Hunsaker et al., 2009; Steffenach et al., 2002), we examined whether inhibition of the Schaffer collateral pathway by activation of Opto-vTrap impairs contextual memory retrieval. We injected the CamKIIα::Opto-vTrap lentivirus into hippocampal CA3 regions unilaterally and implanted an optic cannula into the CA1 region for illumination (Figure 6A). As a vector control without Opto-vTrap, we injected the CMV::mCherry lentivirus. 3 weeks after the surgery, each Opto-vTrap-injected mouse was subjected to contextual fear conditioning on day 1 (Figure 6A). On day 2, each mouse was placed in the same context, where the mouse acquired fear memory for three sessions of 3 min each with a 1-h interval between two sessions (Figure 6B). For activation of Opto-vTrap, we illuminated with 1 mW of continuous blue light during trial 2 for 3 min on day 2 (Figure 6B). As a control condition with no illumination, each mouse was subjected to an additional contextual memory retrieval test on day 3 (Figure 6B). We observed that the freezing behavior was decreased significantly during unilateral activation of Opto-vTrap in trial 2, which was rescued fully 1 h after the laser-off trial 3 (Figures 6C and 6D). In contrast, freezing behavior on day 3 was not changed significantly during trials 4–6 in the absence of illumination (Figures 6B and 6C). The freezing behavior was not changed significantly during trials 1–3 on day 2 in the CMV::mCherry-injected group (Figure 6D). These results indicate that inhibition of the Schaffer collateral pathway by activation of Opto-vTrap can effectively and reversibly impair fear memory retrieval with full recovery within 1 h. We also performed an open field test and novel object recognition test without illumination, and there was no significant difference between the control and Opto-vTrap-expressing group (Figure S5). In addition, we observed that Opto-vTrap can efficiently and reversibly inhibit behavior in a continuous behavioral paradigm (Figure S6). Taken together, these results suggest that Opto-vTrap can be utilized in behaving animals to spatially, temporally, and cell-type-specifically silence the brain circuit and behavior by illumination with fast onset and a fast recovery time.

DISCUSSION

The newly developed Opto-vTrap is a highly effective optogenetic trap for light-induced reversible inhibition of vesicular release, synaptic transmission, gliotransmission, and behavior. By bypassing the membrane potential change and directly targeting the vesicular exocytic machinery, we have been able to circumvent many confounding effects that are known for Arch and NpHR, such as hyperpolarization-induced rebound spikes and residual Ca^{2+} in presynaptic terminals. These unique advantages of Opto-vTrap (i.e., voltage independence and Ca^{2+} independence, indicate its broad applicability not only to neurons but also non-excitable cells such glial cells, endocrine cells, and any other secretory cells that do not express a host of voltage-gated ion channels to mediate action potentials or rebound spikes. Its broad applicability should also include possible uses in *in vitro* models of cell culture and organoid systems, *ex vivo* models of brain slices of various regions, and *in vivo* animal models of behaving animals. These advantages place Opto-vTrap at the top of the list of choices for optogenetic probe for inhibition.

Opto-vTrap has a higher inhibition efficiency than other methods of inhibition of synaptic transmission, such as the G_i-DREADD system. It has been reported previously that locally expressing AAV-hM4Di in the hippocampal CA3 shows an approximately 30% block of field excitatory postsynaptic potential (fEPSP) by bath perfusion of clozapine-N-oxide, the agonist of hM4Di (Kätzel et al., 2014). We observed an approximately 45% block of eEPSCs (Figure 4H) upon activation of Opto-vTrap. In contrast, we observed almost complete inhibition of TFLLR-induced increases in frequency of gFICs and a significant decrease in the frequency of basal gFICs (Figure 5F). It appears that glial vesicular release was almost completely inhibited by activation of Opto-vTrap, whereas synaptic vesicular release was blocked by only half. This discrepancy can be explained when we consider the bilateral projection from CA3 to CA1 in the hippocampus. Hippocampal CA1 inputs come from not only the ipsilateral CA3-CA1 Shaffer collateral pathway but also the contralateral CA3 commissural pathway (Bliss et al., 1983). Moreover, there are some reports showing

Figure 4. Activation of Opto-vTrap inhibits eEPSC in Schaffer collateral synapses

(A) Map of the lentiviral CamKIIα::Opto-vTrap construct and injection strategy for Opto-vTrap expression.

(B) Representative membrane potential trace in response to current injection in Opto-vTrap-expressing cells.

(C) Representative membrane potential trace of Opto-vTrap-expressing cells. A blue line indicates blue light illumination.

(D) Summary graph of membrane potential from before and light on conditions (n = 5, Wilcoxon test).

(E) Experimental scheme of eEPSC recording with blue light illumination and representative traces of eEPSCs in control and Opto-vTrap-injected acute brain slices during before, light on, and after conditions. Scale bar: 20 ms, 100 pA. P1, first-peak amplitude; P2, second-peak amplitude.

(F) Summary bar graph of the first amplitude during paired-pulse stimulation under control (left) and Opto-vTrap conditions (right) (n = 6, control; n = 9, Opto-vTrap).

(G) Percentage of the first amplitude during paired-pulse stimulation in control (left) and Opto-vTrap groups (right). A blue box indicates blue light illumination (0–15 min) (n = 6, control; n = 9, Opto-vTrap).

(H) Summary bar graph of the percentage of the first amplitude during before, light on, and after conditions in control and opto-vTrap groups. n = 7, control; n = 12, Opto-vTrap; ****p < 0.0001, *p < 0.05; not significant (n.s.) between before versus after (25 and 30 min); one-way ANOVA (mixed-effects analysis).

(I) Percentage of the second amplitude during paired-pulse stimulation in control (left) and Opto-vTrap mice (right). A blue box indicates blue light illumination (0–15 min) (n = 7, control; n = 12, Opto-vTrap).

(J) Summary bar graph of the percentage of the second amplitude during before, light on, and after conditions in the control and Opto-vTrap groups. n = 7, control; n = 12, Opto-vTrap. *p < 0.05; n.s. between before versus after (20, 25, and 30 min) in EPSC second amplitude (Figure 4J); one-way ANOVA (mixed-effects analysis).

(K) PPR during paired-pulse stimulation in control (left) and Opto-vTrap groups (right) (n = 7, control; n = 12, Opto-vTrap).

(L) Summary bar graph of the PPR during before, light on, and after conditions in control and Opto-vTrap. n = 7, control; n = 12, Opto-vTrap; n.s. between all conditions, one-way ANOVA (mixed-effects analysis).

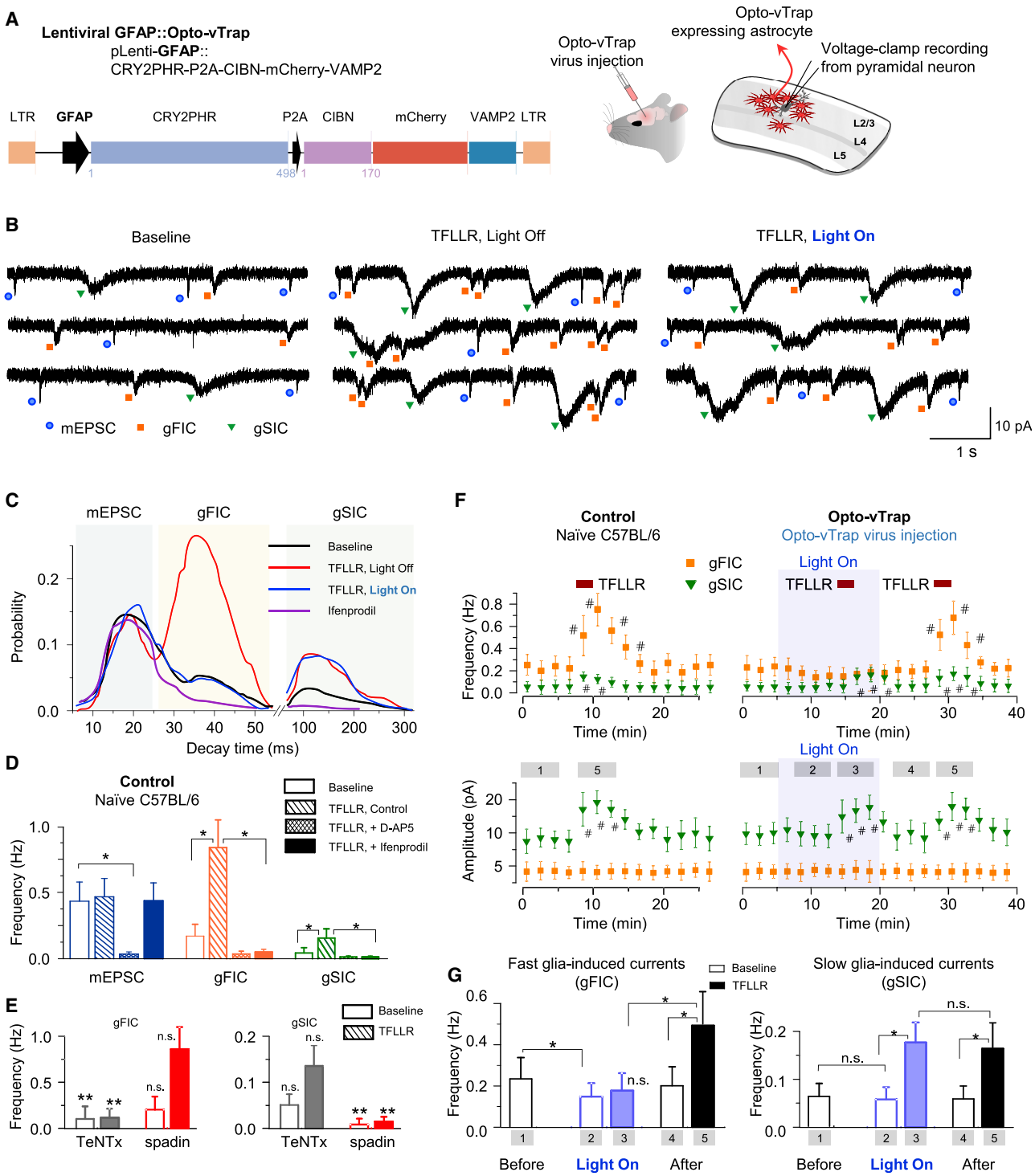

Figure 5. Activation of Opto-vTrap inhibits neocortical astrocytic vesicular gliotransmitter release

(A) Map of the lentiviral GFAP::Opto-vTrap construct and experimental strategy of astrocytic exocytosis-mediated fast inward NMDAR-mediated current measurement.

(B) Representative whole-cell current recording in the baseline, TFLLR application with blue light off, and TFLLR application with light on.

(C) Kinetics of transient NMDAR-mediated currents in the neurons under the GFAP::Opto-vTrap condition.

(D) Pooled data on the frequency before (baseline) and after stimulation of astrocytes with TFLLR in the control (n = 14, control; n = 6, TFLLR+D-AP5; n = 7, TFLLR+ifenprodil; *p < 0.05, paired t test).

(legend continued on next page)

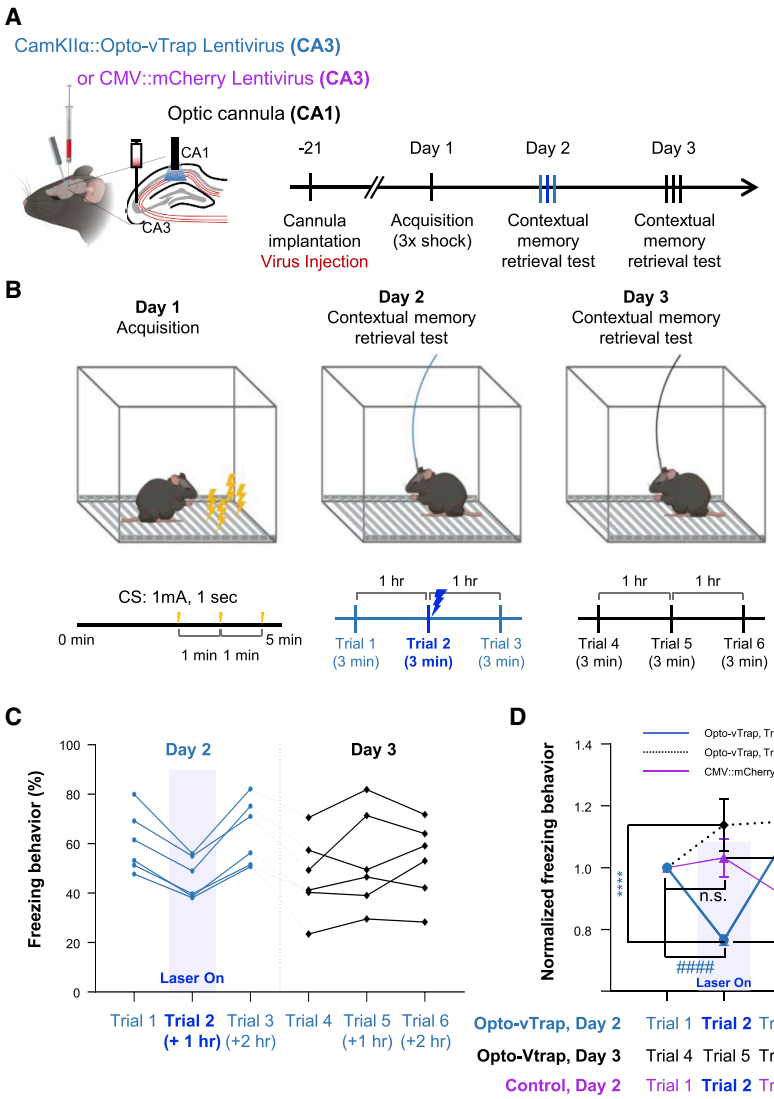

Figure 6. Activation of Opto-vTrap reversibly inhibits contextual fear memory retrieval

(A) Experimental strategy of Schaffer collateral pathway-mediated memory retrieval (fear conditioning test) in opto-vTrap-injected mice.

(B) Experimental scheme of the memory retrieval test. During the contextual retrieval test in trials 1–6, the blue laser was on in trial 2 only.

(C) Percentage of freezing of each Opto-vTrap mouse during trials 1–3 and 4–6. The blue box indicates the timing of 488-nm laser exposure (trial 2 only) (n = 6).

(D) Normalized freezing behavior from (C). Percentages of freezing of trials 1–3 are normalized to trial 1, and those of trials 4–6 are normalized to trial 4 (n = 10, control; n = 6, Opto-vTrap; ****p < 0.0001 in Opto-vTrap trial 2 versus Opto-vTrap trial 5, ***p < 0.001 in Opto-vTrap trial 2 versus control trial 2, 2-way ANOVA; ####p < 0.0001, repeated-measures one-way ANOVA in Opto-vTrap trial 1 versus trial 2. Data are presented as the mean ± SEM).

that ipsilateral and contralateral projections contribute equally to synaptic plasticity in rodent models (Bliss et al., 1983; Kohl et al., 2011; Shipton et al., 2014). Therefore, the partial block of eEPSCs is most likely due to the remaining synaptic release from non-Opto-vTrap-expressing fibers, such as contralateral CA3 commissural projections, during electrical stimulation of the Shaffer collateral pathway in the *stratum radiatum* of the hippocampus. In contrast, the gFIC current, which showed almost complete inhibition by Opto-vTrap activation, occurs only in the local area where Opto-vTrap is expressed. In addition, Opto-vTrap virus transduction efficiency might slightly affect the already high inhibition efficiency.

Thus, we propose that expression and activation of Opto-vTrap can inhibit vesicular release with high efficiency. We also performed a contextual fear memory retrieval test to verify whether Opto-vTrap is applicable to behaving animals. We unilaterally targeted the same CA3-CA1 circuit that was tested by Opto-vTrap with high efficiency in acute brain slices. We observed about 25% block of memory retrieval upon Opto-vTrap activation (Figures 6C and 6D), a relatively lower value than other experimental results. It is well known that various circuits are involved in the contextual memory retrieval process, such as CA3-CA1, CA1-amygdala, or CA1-medial prefrontal cortex (mPFC) (Jimenez et al., 2020; Liu et al., 2012; Orsini et al., 2011; Xu et al., 2016). Given the unilateral inhibition of the CA3-CA1 circuit by Opto-vTrap and the possibility of other circuits being involved during contextual memory retrieval, a 25% block of memory retrieval should be considered significant. Thus, we propose that Opto-vTrap can inhibit a specific circuit with high efficiency in behaving animals.

One of the most prominent advantages of Opto-vTrap is its fast recovery time. After immediate clustering, Opto-vTrap took about 15 min to fully decluster (Figure 2D). The similar 15-min recovery time was observed with vesicular gliotransmission (Figures 5F and 5G). In hippocampal slices, decreased neurotransmission upon Opto-vTrap activation was recovered

(E) Pooled data on the frequency of gFICs and gSICs recorded after intracellular perfusion of astrocytes with tetanus neurotoxin light chain (TeNTx; 3 nM, 15 min prior to recordings) or bath application of spadin (TREK-1 blocker, 200 nM) (n = 6, baseline; n = 5, TFLLR; **p < 0.01, non-paired t test).

(F) Representative time course of the average amplitude and frequency of glia-induced fast currents (gFICs) and glia-induced slow currents (gSICs) recorded in neocortical neurons of control (left) and Opto-vTrap (right) mice. The blue box indicates the timing of blue light illumination (5–20 min) (n = 4, control; n = 4, Opto-vTrap, #p < 0.05, paired t test).

(G) Pooled data on the frequency of gFICs and gSICs during light off, light on, and light-off (n = 4, baseline; n = 4, TFLLR; *p < 0.05, non-paired t test). Data are presented as the mean ± SEM.

within 30 min with a slight but statistically insignificant increase in PPR (Figures 4G–4L). Finally, in the fear memory retrieval test, we observed complete recovery of impaired memory retrieval by activation of Opto-vTrap within 1 h (Figure 6C). Although we could not test shorter intervals because of the nature of the behavioral test, it is possible that the recovery time of behavior could be shorter than 1 h, based on the *in vitro* results (Figures 2D and 5D). It will be interesting to test a shorter recovery time with other behavioral tests that require a shorter interval between two consecutive sessions. Nevertheless, the observed 1-h recovery time of Opto-vTrap is far superior to other optogenetic probes, such as PA-BoNT and InSynC, which have a very long recovery time of about 24 h (Lin et al., 2013; Liu et al., 2019). The critical difference is that activation of Opto-vTrap does not induce protein damage; it would take a long time for damaged proteins to be replenished by *de novo* protein synthesis. Indeed, as a preliminary experiment, we investigated whether inhibition of dopamine release from the terminals of substantia nigra pars compacta (SNpc) neurons at the dorsal striatum by Opto-vTrap causes real-time motor behavior deficits (Figure S6). We observed a significant decrease in moving activities within 10 min of light stimulation and recovery after "light off" (Figures S6C and S6D), although the detailed mechanism of reduction in motion upon Opto-vTrap activation needs future investigation. Such a fast recovery time should provide greater flexibility regarding the types of behavioral tests that can be used with Opto-vTrap.

Another important advantage of Opto-vTrap is the fact that its design is based on LARIAT, which utilizes CIBN and CRY2 interaction upon illumination. Recently, we developed various versions of LARIAT-derived optogenetic tools, such as IM-LARIAT and mRNA-LARIAT (Kim et al., 2020a; Nguyen et al., 2016), in which the basic principle of LARIAT is applied to induce rapid intracellular membrane aggregation and inhibition of translation of specific mRNAs, respectively. Likewise, we have developed a new version of LARIAT-derived Opto-vTrap that inhibits vesicular exocytosis by clustering vesicles through VAMP2, which nonspecifically targets various exocytic vesicles. Based on a similar concept, it should be possible to use different target proteins, such as vGluT, vGAT, and vMAT, to specifically target a subtype of vesicles containing glutamate, GABA, and dopamine, respectively. We expect that not only synaptic transmitter or gliotransmitter release but also dense core vesicle-containing small peptide release could be blocked by Opto-vTrap (Figure 3). We have also developed much-enhanced versions of CRY2 variants for CRY2:CRY2 homodimerization, such as CRY2clust and CRY2^{E281A}-A9 (Park et al., 2017; Kim et al., 2020b). CRY2clust shows enhanced clustering properties compared with the currently used CRY2PHR (Park et al., 2017), whereas CRY2^{E281A}-A9 shows ultra-high light sensitivity to allow non-invasive light stimulation without a need for insertion of fiberoptic cables (Kim et al., 2020b). Adopting these CRY2 variants for Opto-vTrap will be a natural course to take and should enhance the clustering properties and light sensitivity of the existing Opto-vTrap. These exciting possibilities await future investigation.

The basic concepts and molecular tools we developed in this study should be very useful for delineating circuit-level mechanisms of how various brain regions contribute to cognition and behavior. Furthermore, LARIAT-based Opto-vTrap promises future development of new versatile and flexible optogenetic tools.

STAR★METHODS

Detailed methods are provided in the online version of this paper and include the following:

- KEY RESOURCES TABLE
- RESOURCE AVAILABILITY
  - Lead contact
  - Materials availability
  - Data and code availability
- EXPERIMENTAL MODEL AND SUBJECT DETAILS
  - Animals
  - Cell lines
  - Preparation of DNA construct
- METHOD DETAILS
  - Transfection and live-cell imaging
  - Stereotaxic surgery and viral injection
  - Immunohistochemistry of brain slice and super resolution imaging
  - Slice patch-clamp recording
  - Animal behavior test
- QUANTIFICATION AND STATISTICAL ANALYSIS

SUPPLEMENTAL INFORMATION

Supplemental information can be found online at https://doi.org/10.1016/j.neuron.2021.11.003.

ACKNOWLEDGMENTS

This work was supported by the Institute for Basic Science (IBS), Center for Cognition and Sociality (IBS-R001-D2); KAIST Institute for the BioCentury; and National Research Foundation of Korea (NRF-2020R1A2C3014742). This paper is based on research conducted as part of the KAIST-funded Global Singularity Research Program for 2021.

AUTHOR CONTRIBUTIONS

J.W., C.J.L., and W.D.H. designed the study, analyzed the data, and wrote the manuscript. J.W. and S.E.L. performed and analyzed confocal imaging of Opto-vTrap. J.W. performed and analyzed TIRF microscopy imaging. J.W., M.W.J., S.K., and Y.H.J. performed and analyzed membrane potential and eEPSC measurements. Y.P. performed and analyzed NMDAR-mediated spontaneous current measurements. J.W. and A.K. performed and analyzed the fear conditioning behavior test. J.W. and S.P. performed and analyzed the animal motor activity inhibition test. J.W. and S.E.L. designed the viral vector construct.

DECLARATION OF INTERESTS

The authors declare no competing interests.

Received: December 18, 2020
Revised: September 1, 2021
Accepted: November 3, 2021
Published: November 30, 2021

REFERENCES

Amaral, D.G., and Witter, M.P. (1989). The three-dimensional organization of the hippocampal formation: a review of anatomical data. Neuroscience *31*, 571–591.

Arias, N., Méndez, M., and Arias, J.L. (2015). The importance of the context in the hippocampus and brain related areas throughout the performance of a fear conditioning task. Hippocampus *25*, 1242–1249.

Armbruster, B.N., Li, X., Pausch, M.H., Herlitze, S., and Roth, B.L. (2007). Evolving the lock to fit the key to create a family of G protein-coupled receptors potently activated by an inert ligand. Proc. Natl. Acad. Sci. USA *104*, 5163–5168.

Becherer, U., Pasche, M., Nofal, S., Hof, D., Matti, U., and Rettig, J. (2007). Quantifying exocytosis by combination of membrane capacitance measurements and total internal reflection fluorescence microscopy in chromaffin cells. PLoS ONE *2*, e505.

Bliss, T.V., Lancaster, B., and Wheal, H.V. (1983). Long-term potentiation in commissural and Schaffer projections to hippocampal CA1 cells: an in vivo study in the rat. J. Physiol. *341*, 617–626.

Boyden, E.S., Zhang, F., Bamberg, E., Nagel, G., and Deisseroth, K. (2005). Millisecond-timescale, genetically targeted optical control of neural activity. Nat. Neurosci. *8*, 1263–1268.

Bugaj, L.J., Choksi, A.T., Mesuda, C.K., Kane, R.S., and Schaffer, D.V. (2013). Optogenetic protein clustering and signaling activation in mammalian cells. Nat. Methods *10*, 249–252.

Chow, B.Y., Han, X., Dobry, A.S., Qian, X., Chuong, A.S., Li, M., Henninger, M.A., Belfort, G.M., Lin, Y., Monahan, P.E., and Boyden, E.S. (2010). High-performance genetically targetable optical neural silencing by light-driven proton pumps. Nature *463*, 98–102.

Deák, F., Shin, O.H., Kavalali, E.T., and Südhof, T.C. (2006). Structural determinants of synaptobrevin 2 function in synaptic vesicle fusion. J. Neurosci. *26*, 6668–6676.

Dittgen, T., Nimmerjahn, A., Komai, S., Licznerski, P., Waters, J., Margrie, T.W., Helmchen, F., Denk, W., Brecht, M., and Osten, P. (2004). Lentivirus-based genetic manipulations of cortical neurons and their optical and electrophysiological monitoring in vivo. Proc. Natl. Acad. Sci. USA *101*, 18206–18211.

Dobrunz, L.E., and Stevens, C.F. (1997). Heterogeneity of release probability, facilitation, and depletion at central synapses. Neuron *18*, 995–1008.

Fanselow, M.S., and LeDoux, J.E. (1999). Why we think plasticity underlying Pavlovian fear conditioning occurs in the basolateral amygdala. Neuron *23*, 229–232.

Gruart, A., Muñoz, M.D., and Delgado-García, J.M. (2006). Involvement of the CA3-CA1 synapse in the acquisition of associative learning in behaving mice. J. Neurosci. *26*, 1077–1087.

Harada, K., Kamiya, T., and Tsuboi, T. (2016). Gliotransmitter Release from Astrocytes: Functional, Developmental, and Pathological Implications in the Brain. Front. Neurosci. *9*, 499.

Hastoy, B., Scotti, P.A., Milochau, A., Fezoua-Boubegtiten, Z., Rodas, J., Megret, R., Desbat, B., Laguerre, M., Castano, S., Perrais, D., et al. (2017). A Central Small Amino Acid in the VAMP2 Transmembrane Domain Regulates the Fusion Pore in Exocytosis. Sci. Rep. *7*, 2835.

Hayashi, T., McMahon, H., Yamasaki, S., Binz, T., Hata, Y., Südhof, T.C., and Niemann, H. (1994). Synaptic vesicle membrane fusion complex: action of clostridial neurotoxins on assembly. EMBO J. *13*, 5051–5061.

Hollenberg, M.D., Saifeddine, M., al-Ani, B., and Kawabata, A. (1997). Proteinase-activated receptors: structural requirements for activity, receptor cross-reactivity, and receptor selectivity of receptor-activating peptides. Can. J. Physiol. Pharmacol. *75*, 832–841.

Hunsaker, M.R., Tran, G.T., and Kesner, R.P. (2009). A behavioral analysis of the role of CA3 and CA1 subcortical efferents during classical fear conditioning. Behav. Neurosci. *123*, 624–630.

Jimenez, J.C., Berry, J.E., Lim, S.C., Ong, S.K., Kheirbek, M.A., and Hen, R. (2020). Contextual fear memory retrieval by correlated ensembles of ventral CA1 neurons. Nat. Commun. *11*, 3492.

Karpova, A.Y., Tervo, D.G., Gray, N.W., and Svoboda, K. (2005). Rapid and reversible chemical inactivation of synaptic transmission in genetically targeted neurons. Neuron *48*, 727–735.

Kätzel, D., Nicholson, E., Schorge, S., Walker, M.C., and Kullmann, D.M. (2014). Chemical-genetic attenuation of focal neocortical seizures. Nat. Commun. *5*, 3847.

Kennedy, M.J., Hughes, R.M., Peteya, L.A., Schwartz, J.W., Ehlers, M.D., and Tucker, C.L. (2010). Rapid blue-light-mediated induction of protein interactions in living cells. Nat. Methods *7*, 973–975.

Kim, J.J., and Fanselow, M.S. (1992). Modality-specific retrograde amnesia of fear. Science *256*, 675–677.

Kim, N.Y., Lee, S., Yu, J., Kim, N., Won, S.S., Park, H., and Heo, W.D. (2020a). Optogenetic control of mRNA localization and translation in live cells. Nat. Cell Biol. *22*, 341–352.

Kim, S., Kyung, T., Chung, J.H., Kim, N., Keum, S., Lee, J., Park, H., Kim, H.M., Lee, S., Shin, H.S., and Do Heo, W. (2020b). Non-invasive optical control of endogenous Ca^{2+} channels in awake mice. Nat. Commun. *11*, 210.

Kohl, M.M., Shipton, O.A., Deacon, R.M., Rawlins, J.N., Deisseroth, K., and Paulsen, O. (2011). Hemisphere-specific optogenetic stimulation reveals left-right asymmetry of hippocampal plasticity. Nat. Neurosci. *14*, 1413–1415.

Lee, Y., Messing, A., Su, M., and Brenner, M. (2008). GFAP promoter elements required for region-specific and astrocyte-specific expression. Glia *56*, 481–493.

Lee, S., Park, H., Kyung, T., Kim, N.Y., Kim, S., Kim, J., and Heo, W.D. (2014). Reversible protein inactivation by optogenetic trapping in cells. Nat. Methods *11*, 633–636.

Lin, J.Y., Lin, M.Z., Steinbach, P., and Tsien, R.Y. (2009). Characterization of engineered channelrhodopsin variants with improved properties and kinetics. Biophys. J. *96*, 1803–1814.

Lin, J.Y., Sann, S.B., Zhou, K., Nabavi, S., Proulx, C.D., Malinow, R., Jin, Y., and Tsien, R.Y. (2013). Optogenetic inhibition of synaptic release with chromophore-assisted light inactivation (CALI). Neuron *79*, 241–253.

Liu, X., Ramirez, S., Pang, P.T., Puryear, C.B., Govindarajan, A., Deisseroth, K., and Tonegawa, S. (2012). Optogenetic stimulation of a hippocampal engram activates fear memory recall. Nature *484*, 381–385.

Liu, Q., Sinnen, B.L., Boxer, E.E., Schneider, M.W., Grybko, M.J., Buchta, W.C., Gibson, E.S., Wysoczynski, C.L., Ford, C.P., Gottschalk, A., et al. (2019). A Photoactivatable Botulinum Neurotoxin for Inducible Control of Neurotransmission. Neuron *101*, 863–875.e6.

Mahn, M., Prigge, M., Ron, S., Levy, R., and Yizhar, O. (2016). Biophysical constraints of optogenetic inhibition at presynaptic terminals. Nat. Neurosci. *19*, 554–556.

Mattingly, M., Weineck, K., Costa, J., and Cooper, R.L. (2018). Hyperpolarization by activation of halorhodopsin results in enhanced synaptic transmission: Neuromuscular junction and CNS circuit. PLoS ONE *13*, e0200107.

Nagel, G., Szellas, T., Huhn, W., Kateriya, S., Adeishvili, N., Berthold, P., Ollig, D., Hegemann, P., and Bamberg, E. (2003). Channelrhodopsin-2, a directly light-gated cation-selective membrane channel. Proc. Natl. Acad. Sci. USA *100*, 13940–13945.

Nguyen, M.K., Kim, C.Y., Kim, J.M., Park, B.O., Lee, S., Park, H., and Heo, W.D. (2016). Optogenetic oligomerization of Rab GTPases regulates intracellular membrane trafficking. Nat. Chem. Biol. *12*, 431–436.

Orsini, C.A., Kim, J.H., Knapska, E., and Maren, S. (2011). Hippocampal and prefrontal projections to the basal amygdala mediate contextual regulation of fear after extinction. J. Neurosci. *31*, 17269–17277.

Park, H., Kim, N.Y., Lee, S., Kim, N., Kim, J., and Heo, W.D. (2017). Optogenetic protein clustering through fluorescent protein tagging and extension of CRY2. Nat. Commun. *8*, 30.

Parpura, V., and Zorec, R. (2010). Gliotransmission: Exocytotic release from astrocytes. Brain Res. Brain Res. Rev. *63*, 83–92.

Raimondo, J.V., Kay, L., Ellender, T.J., and Akerman, C.J. (2012). Optogenetic silencing strategies differ in their effects on inhibitory synaptic transmission. Nat. Neurosci. *15*, 1102–1104.

Rizo, J., and Xu, J. (2015). The Synaptic Vesicle Release Machinery. Annu. Rev. Biophys. *44*, 339–367.

Rosenfeldt, G., Viana, R.M., Mootz, H.D., von Arnim, A.G., and Batschauer, A. (2008). Chemically induced and light-independent cryptochrome photoreceptor activation. Mol. Plant *1*, 4–14.

Saloman, J.L., Scheff, N.N., Snyder, L.M., Ross, S.E., Davis, B.M., and Gold, M.S. (2016). Gi-DREADD Expression in Peripheral Nerves Produces Ligand-Dependent Analgesia, as well as Ligand-Independent Functional Changes in Sensory Neurons. J. Neurosci. *36*, 10769–10781.

Schoch, S., Deák, F., Königstorfer, A., Mozhayeva, M., Sara, Y., Südhof, T.C., and Kavalali, E.T. (2001). SNARE function analyzed in synaptobrevin/VAMP knockout mice. Science *294*, 1117–1122.

Schoenenberger, P., Schärer, Y.P., and Oertner, T.G. (2011). Channelrhodopsin as a tool to investigate synaptic transmission and plasticity. Exp. Physiol. *96*, 34–39.

Shipton, O.A., El-Gaby, M., Apergis-Schoute, J., Deisseroth, K., Bannerman, D.M., Paulsen, O., and Kohl, M.M. (2014). Left-right dissociation of hippocampal memory processes in mice. Proc. Natl. Acad. Sci. USA *111*, 15238–15243.

Söllner, T., Bennett, M.K., Whiteheart, S.W., Scheller, R.H., and Rothman, J.E. (1993). A protein assembly-disassembly pathway in vitro that may correspond to sequential steps of synaptic vesicle docking, activation, and fusion. Cell *75*, 409–418.

Steffenach, H.A., Sloviter, R.S., Moser, E.I., and Moser, M.B. (2002). Impaired retention of spatial memory after transection of longitudinally oriented axons of hippocampal CA3 pyramidal cells. Proc. Natl. Acad. Sci. USA *99*, 3194–3198.

Sudhof, T.C. (2004). The synaptic vesicle cycle. Annu. Rev. Neurosci. *27*, 509–547.

Südhof, T.C. (2012). Calcium control of neurotransmitter release. Cold Spring Harb. Perspect. Biol. *4*, a011353.

Weiss, N., Zamponi, G.W., and De Waard, M. (2012). How do T-type calcium channels control low-threshold exocytosis? Commun. Integr. Biol. *5*, 377–380.

Wiegert, J.S., Mahn, M., Prigge, M., Printz, Y., and Yizhar, O. (2017). Silencing Neurons: Tools, Applications, and Experimental Constraints. Neuron *95*, 504–529.

Woo, D.H., Han, K.S., Shim, J.W., Yoon, B.E., Kim, E., Bae, J.Y., Oh, S.J., Hwang, E.M., Marmorstein, A.D., Bae, Y.C., et al. (2012). TREK-1 and Best1 channels mediate fast and slow glutamate release in astrocytes upon GPCR activation. Cell *151*, 25–40.

Xu, C., Krabbe, S., Gründemann, J., Botta, P., Fadok, J.P., Osakada, F., Saur, D., Grewe, B.F., Schnitzer, M.J., Callaway, E.M., and Lüthi, A. (2016). Distinct Hippocampal Pathways Mediate Dissociable Roles of Context in Memory Retrieval. Cell *167*, 961–972.e16.

Zhang, F., Wang, L.P., Brauner, M., Liewald, J.F., Kay, K., Watzke, N., Wood, P.G., Bamberg, E., Nagel, G., Gottschalk, A., and Deisseroth, K. (2007). Multimodal fast optical interrogation of neural circuitry. Nature *446*, 633–639.

Zhou, Q., Zhou, P., Wang, A.L., Wu, D., Zhao, M., Südhof, T.C., and Brunger, A.T. (2017). The primed SNARE-complexin-synaptotagmin complex for neuronal exocytosis. Nature *548*, 420–425.

STAR★METHODS

KEY RESOURCES TABLE

REAGENT or RESOURCE	SOURCE	IDENTIFIER
Antibodies		
Anti-mCherry antibody	Abcam	ab167453; RRID:AB_2571870
Anti-Bassoon antibody (SAP7F407)	Novus Biologicals	NB120-13249; RRID:AB_2066978
Anti-SYT1 antibody	Abcam	ab133856; RRID:AB_2885088
Bacterial and virus strains		
Lenti-CamKIIα::CRY2PHR-P2A-CIBN-mCherry-VAMP2	IBS Virus Facility; KIST Virus Facility	Lentiviral CamKIIα::Opto-vTrap
Lenti-GFAP::CRY2PHR-P2A-CIBN-mCherry-VAMP2	IBS Virus Facility; KIST Virus Facility	Lentiviral GFAP::Opto-vTrap
Lenti-CMV::mCherry	IBS Virus Facility	N/A
AAV-CK(0.4)::CRY2PHR-P2A-CIBN-mCherry-VAMP2	IBS Virus Facility	AAV CK(0.4)::Opto-vTrap
Lenti-DDC::CRY2PHR-P2A-CIBN-mCherry-VAMP2	KIST Virus Facility	Lentiviral DDC::Opto-vTrap
Recombinant DNA		
pcDNA3.1-CMV::CIBN-mCherry-VAMP2	Addgene	pcDNA3.1-CMV-CIBN-mCherry-VAMP2 (ID# 178573)
pcDNA3.1-CMV::CRY2PHR-mCitrine	Park et al., 2017	N/A
pLenti-CamKIIα::CRY2PHR-P2A-CIBN-mCherry-VAMP2	Addgene	pLenti-CamKIIα-CRY2PHR-P2A-CIBN-mCherry-VAMP2 (ID# 178574)
pLenti-GFAP::CRY2PHR-P2A-CIBN-mCherry-VAMP2	Addgene	pLenti-GFAP-CRY2PHR-P2A-CIBN-mCherry-VAMP2 (ID# 178575)
pAAV-CK(0.4)::CRY2PHR-P2A-CIBN-mCherry-VAMP2	Addgene	pAAV-CK(0.4)-CRY2PHR-P2A-CIBN-mCherry-VAMP2 (ID# 178576)
Software and algorithms		
Clampfit	Molecular Devices	pClamp; RRID: SCR_011323
GraphPad Prism 7	GraphPad software	GraphPad Prism; RRID: SCR_002798
ImageJ	National Institutes of Health	ImageJ; RRID: SCR_003070
NIS-Elements	Nikon	NIS-Elements; RRID: SCR_014329
Mini Analysis Program, RRID:SCR_002184	Synaptosoft	Mini Analysis Program; RRID: SCR_002184
Ethovision XT	Noldus	EthoVision XT; RRID: SCR_000441
FreezeFrame/Freezeview	Coulbourn Instruments	FreezeFrame; RRID: SCR_014429

RESOURCE AVAILABILITY

Lead contact

Further information and requests for resources and reagents should be directed to and will be fulfilled by the Lead Contact Won Do Heo (wondo@kaist.ac.kr).

Materials availability

The plasmids for pcDNA3.1-CMV::CIBN-mCherry-VAMP2 (#178573, Addgene), pLenti-CamKIIα::CRY2PHR-P2A-CIBN-mCherry-VAMP2 (#178574, Addgene), pLenti-GFAP::CRY2PHR-P2A-CIBN-mCherry-VAMP2 (#178575, Addgene), pAAV-CK(0.4)::CRY2PHR-P2A-CIBN-mCherry-VAMP2 (#178576, Addgene) are deposited to Addgene. The viruses generated in this study (#Lentiviral CamKIIα::Opto-vTrap; #Lentiviral GFAP::Opto-vTrap, #AAV CK(0.4)::Opto-vTrap; and Lentiviral DDC::Opto-vTrap) are available from IBS Virus Facility.

Data and code availability

Any additional information required to reanalyze the data reported in this work paper is available from the Lead Contact upon request.

EXPERIMENTAL MODEL AND SUBJECT DETAILS

Animals

For electrophysiology in brain acute slice, male C57BL/6J mice (6-10-week-old) were used. For behavioral test, male C57BL/6J (10-14-week-old) were used. All mice were maintained by trained facaulty of departmental animal facility, with 12:12-h light–dark cycle (lights on 8:00 A.M.) and free access to rodent chow and reverse osmotic water. All experimental procedures were conducted in accordance with the Institutional Animal Care and Use Committee (IACUC) of Korea Institute of Science and Technology (Seoul, Korea) and Institute of Basic Science (Deajeon, Korea).

Cell lines

For the *in vitro* imaging, COS-7 cells (#21651, Korean Cell Line Bank) and Neuroscreen-1 cells (NS-1, subclone of PC12 cells; Cellomics) were used. COS-7 cells were maintained in 90% Dulbecco's modified Eagle's medium (DMEM, #10-013-CV, Corning) with 10% heat-inactivated fetal bovine serum (FBS, #10082147, GIBCO, Life technologies) at 37°C and 10% CO_2. NS-1 cells were provided by T. Meyer (Stanford University) and maintained in 80% Ham's F-12K (Kaighn's) Medium (#21127022, GIBCO, Life technologies) with 15% heat-inactivated horse serum (#26050088, GIBCO, Life technologies) and 5% heat-inactivated FBS (#10082147, GIBCO, Life technologies) at 37°C and 5% CO_2. All cell lines were confirmed to be free from mycoplasma by using e-Myco Mycoplasma PCR detection kit (ver. 2.0, iNtRON).

Preparation of DNA construct

Mus musculus VAMP2 containing vector (VAMP2-BTX) was provided by J. Sanes (Harvard University). CRY2PHR-mCherry and CIBN-pmEGFP coding vectors were provided by C.L.Tucker (University of Colorado). For cloning the CIBN-mCherry-VAMP2 construct, sequence encoding CIBN (amino acid 1-170 of CIB1) and VAMP2 are PCR-amplified and restricted by NheI/AgeI and XhoI/EcoRI, respectively. The enzyme restricted CIBN and VAMP2 were inserted into corresponding sites of EGFP-C1 vector (Clontech). For cloning the PHR-mCitrine construct, we used a codon-optimized PHR (amino acids 1-498 of CRY2), which has been described in the previous paper (Lee et al., 2014; Nguyen et al., 2016). NheI/AgeI-restricted Codon-optimized PHR are inserted into corresponding sites of pmcitrine-C1 (Clontech). For cloning the PHR-iRFP682 construct, we replaced mCitrine with iRFP682 from iRFP682-N1 vector (Clontech) in PHR-mCitrine construct. For cloning the PHR-P2A-CIBN-mCherry-VAMP2, we amplified PHR and CIBN-mCherry-VAMP2, respectively, with a tagging P2A sequence. PCR-amplified and P2A sequence containing fragments were recombinant with NheI/XhoI restricted pECFP-C1 vector (Clontech) with In-Fusion HD Cloning Kit (#639649, Clontech). For cloning pLenti-CamkIIα-PHR-P2A-CIBN-mCherry-VAMP2, we first cloning pAAV-CamIIa-PHR-P2A-CIBN-mCherry-VAMP2 by inserting AscI/NheI restricted PHR-P2A-CIBN-mCherry-VAMP2 into corresponding sites of pAAV-CaMKIIα-eArchT3.0-P2A-EGFP-WPRE-hGHpA (Clonetech). PCR-amplified CamKIIα-PHR-P2A-CIBN-mCherry-VAMP2 was recombinant with PacI/EcoRI restricted pLenti-CaMKIIα-ChETA-EYFP vector (Clontech) with In-Fusion HD Cloning Kit (#639649, Clontech). For cloning AAV-CK(0.4)- PHR-P2A-CIBN-mCherry-VAMP2, PCR-amplified CK(0.4) from AAV-CK(0.4)GW (Stratagene) was enzymatic liagted with MluI/NheI restricted pAAV-pAAV-CamIIa-PHR-P2A-CIBN-mCherry-VAMP2. For cloning pLenti-GFAP-PHR-P2A-CIBN-mCherry-VAMP2, PacI/BamHI restricted PCR-amplified GfaABC1D promoter was inserted into corresponding sites pLenti-CamKIIα-PHR-P2A-CIBN-mCherry-VAMP2. For cloning pLenti-DDC-PHR-P2A-CIBN-mCherry-VAMP2, MluI/NheI restricted PCR-amplified DDC promoter was inserted into corresponding sites pLenti-CamKIIα-PHR-P2A-CIBN-mCherry-VAMP2.

METHOD DETAILS

Transfection and live-cell imaging

For confocal live-cell imaging, COS-7 cells were transfected by electroporation (Neon Transfection System, Invitrogen) followed by the manufacturer's recommendations. In brief, 1×10^6 COS-7 cells were mixed with a total of 1 μg DNA and electroporated by 2 pulses of 1050 V for 30 msec. 5×10^4 of transfected cells were plated onto each μ-Plate 96 Well ibiTreat well (ibidi, 89626). After the transfection, we covered the plate with aluminum foil to prevent exposure to the light before the experiment. After 20-24 hours, we replace to fresh media and imaging. Live-cell confocal imaging was performed by using a Nikon A1R confocal microscope mounted onto a Nikon Eclipse Ti body and equipped with a CFI Plan Apochromat VC objectives (60×, numerical aperture (NA) 1.4, oil, Nikon Instruments). A Live-cell imaging chamber and incubation system were used for maintaining environmental conditions at 37°C and 10% CO_2 (Live Cell Instruments). Images were acquired and processed by using (NIS-element AR, Nikon Instruments) and light stimulation was performed with a 488-nm laser with around 6.5 μW laser power. For image analysis, NIS-element (Nikon) and ImageJ software were used. Puncta signal was defined as 0.3-2.0 micron square size, circularity 0.0-1.0 in NIS-element (Nikon).

For TIRF imaging, 5×10^4 of NS-1 cells were plated on 8-well Lab-Tek II Chambered Coverglass (#155409, Thermo Scientific) and transfected by Lipofectamine LTX (Invitrogen) followed by manufacturer's recommendations. In brief, a dilute total of 0.2 μg DNA into 20 μL Opti-MEM I Reduced Serum Medium (#31985062, GIBCO, Life technologies) were mixed with Lipofectamine LTX reagent. And then, the DNA and reagent mixture was carefully added with fresh media into each well. After the transfection, we covered the plate with aluminum foil to prevent exposure to the light before the experiment. After 20-24 hours, we replace to fresh media and imaging. TIRF imaging was performed at room temperature (25°C) by using a Nikon Ti-E TIRF microscope equipped with a CFI Apochromat

TIRF 60 × objective (Nikon Instruments). 488-nm laser (CVI-Melles Griot) was used to visualize neuropeptide Y-VENUS and light stimulation, simultaneously. To induce exocytosis, high-KCl containing Ringer's solution (70 mM KCl, 67 mM NaCl, 1 mM MgCl2, 2 mM CaCl2, 10 mM HEPES, and 2.8 mM glucose) was treated into imaging well.

Stereotaxic surgery and viral injection

All viruses were generated from the KIST Virus Facility (http://virus.kist.re.kr) or IBS Virus Facility (http://www.ibs.re.kr/virusfacility). For the viral injection for electrophysiology, mice were anesthetized with 300 mg/kg body weight of 2,2,2-tribromoethanol (#T48402, Sigma-Aldrich). Lentivirus of Lenti-CamKIIα::PHR-P2A-CIBN-mCherry-VAMP2 or AAV-DDC::PHR-P2A-CIBN-mCherry-VAMP was stereotactically injected into the hippocampal CA3 regions (for 6-7-week-old mice, −1.94 mm lambda from bregma, ± 2.28 mm lateral to the midline, −2.10 mm ventral from the brain surface) by using SP100IZ syringe pump (WPI). Lenti-GFAP::PHR-P2A-CIBN-mCherry-VAMP2 was stereotactically injected into the neocortes layer 2/3. For the behavior experiment with optic stimulation, mice were first anesthetized with 4% of isoflurane and oxygen mixture, and re-anesthetized with 20 mg/kg body weight of ketamine. A heating pad was used to maintain body temprature at 36°C. Lentivirus of Lenti-CamKIIα::PHR-P2A-CIBN-mCherry was stereotactically injected into the hippocampal CA3 regions (for 8-10-week-old mice, −1.94 mm lambda from bregma, ± 2.3 mm lateral to the midline, −2.12 mm ventral from the brain surface) by using pressure (Picospritzer III, Parker Hannifin Corp.). Lentivirus of Lenti-DDC::PHR-P2A-CIBN-mCherry was stereotactically injected into the SNpc regions (for 7-9-week-old mice, −3.2 mm lambda from bregma, ± 1.7 mm lateral to the midline, −3 mm ventral from the brain surface) by using syringe pump (KD Scientific). The optic cannula (R-FOC-L100C-22NA, ceramic ferrule-Ø1.25mm/100um/0.22NA, RWD) was targeted to the hippocampal CA1 regions (−1.94 mm lambda from bregma, ± 1.3 mm lateral to the midline, −1.20 mm ventral from the brain surface). After optic cannula implatation, dental cement was applied to cover the skull.

Immunohistochemistry of brain slice and super resolution imaging

For immunostaining, mice were anesthetized with intraperitoneal injection of 2% of 2, 2, 2-Tribromoethanol and perfused with 0.9% of normal saline, followed by ice-cold 4% paraformaldehyde (PFA). Extracted brains were postfixed in 4% of PFA at 4°C during 24 hr followed by dehydrogenized in 30% sucrose containing PBS during 24 hr. Brain slices were prepared as 30 μm thickness by a cryostat and stored in storage solution at 4°C. Brain slices were washed in PBS and incubated in blocking solution (0.3% Triton X-100, 2% donkey serum, 2% goat serum, in 0.1M of PBS) for 1 hr. Brain slices were immunostained in primary antibodies (ab167453, Anti-mCherry antibody, abcam; NB120-13249, Novus Biologicals, anti-Bassoon antibody (SAP7F407); ab133856, Anti-SYT1 antibody, abcam) containing blocking solution on shaker at 4°C during 18 hr. After primary immunostaining, slices were washed in PBS at room and second immunostained in corresponding fluorescence-conjugating secondary antibodies containing blocking solution during 1 hr and then washed in PBS. Brain sections were mounted with fluorecent mounting media (S3023, Dako). A series of fluorescent images were obtained with an Eylra 7 Zeiss super resolution microscope. 3D imaging rendering and analysis were performed by IMARIS software.

Slice patch-clamp recording

For the eEPSC recording, mice were anesthetized with isoflurane and decapitated. The 300 μm coronal slices of hippocampus were prepared in ice-cooling sucrose-based cutting solution (sucrose, 234 mM; KCl, 2.5 mM; MgSO4, 10 mM; NaH2PO4, 1.25 mM; NaHCO3, 24 mM; CaCl2-2H2O, 0.5 mM; and glucose, 11 mM) on D.S.K Linear Slicer pro7 (Dosaka EM Co., Ltd). For evoked-EPSC recording, slices were recovered for at least 1 hour before recording in oxygenated aCSF (NaCl, 126 mM; NaHCO3, 24 mM; KCl, 2.5 mM; NaH2PO4, 1mM; MgCl2, 2 mM; and glucose, 10 mM). For miniature EPSC recording, 1 μM of TTX was added to oxygeneated aCSF. For evoked EPSC and miniature EPSC recording, current was recorded under oxygenated aCSF solution by whole-cell voltage-clamp. Recording electrode (5-8 MΩ) was fabricated standard-wall borosilicate glass (GC150F-10, Warner Instrument Corp., USA) and filled with an $CeMeSO_4$-based internal solution ($CeMeSO_4$, 132 mM; NaCl, 8 mM; HEPES, 10 mM; EGTA, 0.25 mM; Mg-ATP, 2 mM; and Na_2-GTP, 0.5 mM; QX-314, 1 mM; with pH adjusted to 7.3 and osmolality adjusted to 295 mOsmol/kg). Synaptic activity was evoked by paired-stimulus of Schaffer collateral pathway (0.1 ms, 50 mA∼500 mA, 100 msec interval) using a tungsten bipolar electrode holding at −60 mV).

For the membrane potential recording, mice were anesthetized with isoflurane and decapitated. The 300 μm coronal slices of hippocampus were prepared in ice-cooling NMDG-based cutting solution (NMDG, 93 mM; KCl, 2.5 mM; NaH2PO4, 1.2 mM; NaHCO3, 30 mM; HEPES, 20 mM; Glucose, 25 mM; Sodium ascorbate, 5 mM; Thourea, 2 mM; Sodium pyruvate, 3 mM; $MgCl_2$, 10 mM; $CaCl_2$, 0.5 mM, pH adjust to 7.3 with HCl, 310 mOsm). Slices were recovered 15 minutes at 32°C in the same solution. For current injection, current was injected from −100 pA, −20 pA increment upto +100 pA. Membrane potential was recorded under oxygenated aCSF solution. Recording electrodes (5-8 MΩ) was fabricated standard-wall borosilicate glass (GC150F-10, Warner Instrument Corp., USA) and filled with an K-gluconate-based internal solution (120 mM potassium gluconate; 10 mM KCl; 1 mM MgCl2; 0.5 mM EGTA; 40 mM HEPES; with pH adjusting to 7.2 and osmolality adjusting to 300 mOsmol/kg). All recordings are performed at room temperature (25°C).

Animal behavior test

For the contextual fear memory retrieval test, 11-13-weeks-old male mice were individually placed in fear conditioning chambers (Coulbourn Instruments). After a 2.5 min habituation period, a 1 s foot shock (1 mA) was delivered every 1 minute for 2.5 min (total,

3 times shocks) on Day 1. To assess fear contextual memory, the mice were placed back into the same chamber 24 hr after acquisition (Day 2). During all trials of contextual memory retrieval test, optic fiber was connected to optic cannula which was implanted into hippocampal CA1 regeions. On Day 2, contextual fear retrieval test was carried out 3 times (trial 1-3) in 1 hour interval. 1.0 mW of 488 nm laser was turned on only in trial 2. On Day 3, contextual fear retrieval test was carried out 3 times (trial 4-6) without laser. The behavior of the mice was recorded with the Freezeframe software (Coulbourn Instruments) and analyzed with Freezeview software (Coulbourn Instruments). For open field test, 10-12-weeks-old male mice were individually placed in white acryl container (40 cm × 40 cm × 40 cm) and allowed to freely move to chamber for 10 minutes for habituation. Animals were allowed to freely explore the apparatus for 10 minutes. The open field was divided into a central zone (12 cm × 12 cm) and a peripheral zone and traveled distance and velocity were analyzed using Ethovision XT software (Noldus). For novel place recognition test, 10-12-weeks-old male mice were individually placed in white acryl container (40 cm × 40 cm × 40 cm) with two identical objects positioned in the first and the second quadrant of the cage (Figure S5) and allowed to freely explore to the objects for 10 minutes (familiarization session). Then, mice were transferred to their home cage for 1 hour. After 1 hour, mice were re-placed to acryl container with two identical objects positioned in the first and the fourth quadrant of the cage (Figure S5D) and allowed to freely explore the objects for 10 minutes (test session). The exploration behavior of each mice was monitored by a video camera and analyzed manually by an experimenter.

QUANTIFICATION AND STATISTICAL ANALYSIS

All analyses were done blindly. The number of experimental samples, mean and SEM values are listed in Figure legends. The numbers and individual dots refer to the number of cells unless otherwise clarified in figure legends. For data presentation and statistical analysis, Graphpad Prism (GraphPad Software) was used. For analyze for electrophysiology, Clampfit (Molecular Devices) and Mini analysis (Synaptosoft) were used. For behavioral analysis, Ethovision XT (Noldus) and Freezeview(Coulbourn Instruments) were used. For image analysis, NIS-element (Nikon) and Imagej software were used. Statistical significance was set at $^{*}p < 0.05$, $^{**}p < 0.01$, $^{***}p < 0.001$, $^{****}p < 0.0001$. Data are presented as mean ± SEM.